Theoretical and numerical analysis of the Dirichlet-to-Neumann map in EIT

Joonas Syren

1.6.2016

HELSINGIN YLIOPISTO — HELSINGFORS UNIVERSITET — UNIVERSITY OF HELSINKI

Tiedekunta/Osasto — Fakultet/Sektion — Faculty	Laitos — Institution — Department
Faculty of Science	Department of Mathematics and Statistics

Tekijä — Författare — Author
Joonas Syren

Työn nimi — Arbetets titel — Title

Theoretical and numerical analysis of the Dirichlet-to-Neumann map in EIT

Oppiaine — Läroämne — Subject
Mathematics

Työn laji — Arbetets art — Level	Aika — Datum — Month and year	Sivumäärä — Sidoantal — Number of pages
Master's Thesis	June 2016	49

Tiivistelmä — Referat — Abstract

In this thesis we consider the Dirichlet-to-Neumann map in Electrical Impedance Tomography (EIT). EIT is a tomography method which uses electrical currents and voltages to determine the conductivity distribution inside the measured object. The Dirichlet-to-Neumann map (DN map) takes the voltage on the boundary and gives the resulting current density on the boundary. This map can be approximated by a matrix known as the Dirichlet-to-Neumann matrix. In this thesis we analyse this matrix using Principal Component Analysis (PCA).

In chapter 1 we give a short introduction to EIT with a brief history of the study and some applications of the method. The Dirichlet-to-Neumann map is derived in chapter 2. Constructing the DN map requires solving the Dirichlet problem which is derived from Maxwell?s equations. The Dirichlet problem and its solvability is studied in this chapter as well. Some of the concepts needed in this study can be found from the appendices.

The method used for approximating the DN map is introduced in chapter 3. The approximated matrices are then analysed using PCA, which is described in the same chapter. PCA can be used to find the components where the variation is the largest and to reduce the dimension of the data using these components. We use a method known as Singular Value Decomposition (SVD) to reduce the dimension of the data and to compute the principal values and components.

We computed the DN matrices with simulated data using different conductivity distributions. We chose the unit circle as our domain with a constant conductivity on the background and four anomalies with changing conductivity. The 4th chapter introduces the computations and the obtained results. The resulting principal components and values are shown in this chapter. An approximation of the data was made using the dimensionality reduction method described in chapter 3. The relative errors for different reconstructions are also shown in chapter 4.

In the final chapter we discuss the results. Our goal was to find out how the four variables in the conductivity distributions affect the dimension of the hyperplane that the DN matrices form. It seems that even with four degrees of freedom the DN matrices vary most on a 2-dimensional plane. We also found out that in this case most of the principal components have almost no effect on the data.

Avainsanat — Nyckelord — Keywords
Inverse Problems, EIT, Principal Component Analysis

Säilytyspaikka — Förvaringsställe — Where deposited
Kumpulan tiedekirjasto

Muita tietoja — Övriga uppgifter — Additional information

HELSINGIN YLIOPISTO — HELSINGFORS UNIVERSITET — UNIVERSITY OF HELSINKI

Tiedekunta/Osasto — Fakultet/Sektion — Faculty	Laitos — Institution — Department
Matemaattis-luonnontieteellinen tiedekunta	Matematiikan ja tilastotieteen laitos

Tekijä — Författare — Author
Joonas Syren

Työn nimi — Arbetets titel — Title

Theoretical and numerical analysis of the Dirichlet-to-Neumann map in EIT

Oppiaine — Läroämne — Subject		
Matematiikka		
Työn laji — Arbetets art — Level	Aika — Datum — Month and year	Sivumäärä — Sidoantal — Number of pages
Pro gradu -tutkielma	Kesäkuu 2016	49 s.

Tiivistelmä — Referat — Abstract

Tässä tutkielmassa käsitellään Dirichlet-to-Neumann -kuvausta Impedanssitomografiassa (EIT). Impedanssitomografia on kuvantamismenetelmä, jossa mitattavan objektin johtavuusjakauma yritetään päätellä sähkövirran ja jännitteen reuna-arvojen avulla. Dirichlet-to-Neumann -kuvaus kuvaa jännitteen reunalla virrantiheydeksi reunalla. Tätä kuvausta voidaan approksimoida matriisilla, jota kutsutaan Dirichlet-to-Neumann matriisiksi. Tässä tutkielmassa analysoimme tätä matriisia käyttämällä pääkomponenttianalyysiä (PCA).

Luvussa 1 on lyhyt johdanto impedanssitomografiaan sekä sen tutkimuksen historiaan. Luvussa esitellään myös muutamia menetelmän sovelluksia. Dirichlet-to-Neumann-kuvauksen määritelmä esitellään luvussa 2. Kuvausta määriteltäessä joudumme ratkaisemaan nk. Dirichlet?n ongelman joka seuraa suoraan Maxwellin yhtälöistä. Tässä luvussa tutkitaan myös Dirichlet?n ongelmaa sekä sen ratkeavuutta. Joitain tässä osiossa tarvittavista käsitteistä löytyy tutkielman lopussa sijaitsevista liitteistä.

Menetelmä, jota käytetään Dirichlet-to-Neumann -kuvauksen approksimointiin esitellään luvussa 3. Saatuja matriiseja analysoidaan käyttämällä pääkomponenttianalyysia, jonka toiminta käydään läpi samassa luvussa. Pääkomponenttianalyysiä voidaan käyttää niiden komponenttien etsimiseen, joiden suuntaan data varioi eniten sekä dimension pienentämiseeen käyttämällä näitä komponentteja. Käytämme singulaariarvohajotelmaa (SVD) datan dimension pienentämiseen sekä laskemaan pääkomponentit sekä näitä vastaavat ominaisarvot.

Laskimme Dirichlet-to-Neumann matriiseja simuloidusta datasta käyttämällä eri johtavuusjakaumia. Laskuissa käytettiin tutkittavana joukkona yksikköympyrää, joka sisältää neljä poikkeamaa, joissa johtavuus muuttuu sekä taustan, jossa johtavuus on vakio. Neljännessä luvussa esitellään suoritetut laskut sekä saadut tulokset. Saadut pääkomponentit sekä niitä vastaavat ominaisarvot löytyvät tästä luvusta. Dataa approksimoitiin käyttämällä dimension pienentämistä menetelmällä, joka kuvaillaan luvussa 3. Eri approksimaatioiden suhteelliset virheet löytyvät luvusta 4.

Viimeisessä luvussa pohditaan tuloksia. Tutkielman tavoitteena oli selvittää miten neljä muuttujaa johtavuusjakaumassa vaikuttavat Dirichlet-to-Neumann matriisien muodostaman hyperpinnan ulottuvuuteen. Laskujen perusteella vaikuttaa siltä, että vaikka johtavuusjakaumissa on neljä vapausastetta, niin Dirichlet-to-Neumann matriisit varioivat lähinnä 2-ulotteisessa avaruudessa. Lisäksi huomattiin, että suurimmalla osalla pääkomponenteista ei ole juurikaan vaikutusta dataan.

Avainsanat — Nyckelord — Keywords
Inversio-ongelmat, Impedanssitomografia, Pääkomponenttianalyysi

Säilytyspaikka — Förvaringsställe — Where deposited
Kumpulan tiedekirjasto

Muita tietoja — Övriga uppgifter — Additional information

This thesis is dedicated to my best friend Leevi

Contents

Chapter 1

Introduction to EIT

Electrical impedance tomography or EIT is an imaging technique which uses electrical currents to determine the inner structure of an object. An electrical current is applied on the surface of the object and the resulting voltage is measured and used to determine the conductivity distribution inside the object.

Determining the condutivity distribution from boundary mesurements is a nonlinear and severely ill-posed inverse problem. An inverse problem is the opposite of a direct problem where we wish to find an effect for a cause. In inverse problems the causality is reversed and we wish to recover the cause with a given effect. The definition of a well-posed problem was given by Jacques Hadamard. A problem is well posed if it has the following properties

(i) A solution to the problem exists

(ii) The solution is unique

(iii) The solution depends continuously on the data.

We can assume that the first condition is true. Clearly the object has a conductivity distribution. The second condition means that having a complete set of boundary measurements of voltage and current determines a unique conductivity. This has been studied thoroughly and is true under a variety of smoothness assumptions. However, the third condition poses a real problem. It can be shown that under certain conditions there can exist arbitrarily large changes in the conductivity distribution which do not have an effect on the boundary data.

This study focuses on the direct problem rather than the inverse problem, using a given conductivity distribution inside the object to determine the voltage and current density on the boundary. Therefore, many different aspects of inverse problems are not included in the theory.

1.1 A brief history of EIT

The foundation for the study of the inverse conductivity problem was laid by Alberto Calderón in his paper in 1980 [15]. Calderón provided a mathematical formulation of the problem which is often referred to as the Calderón problem: "Is it possible to determine the conductivity distribution by making voltage and current measurements on the boundary?"

In 1987 John Sylvester and Gunther Uhlmann [16] provided a fundamental uniqueness result for the problem using Complex geometrical optics. The result implies that a C^2 conductivity distribution inside the object is fully determined by the voltage and current measurements on the boundary in 3 or more dimensions.

In 1996 Adrian Nachman [17] proved uniqueness for the 2-dimensional case with C^2 conductivities and infinite precision data and provided a reconstruction method for this case. A numerical implementation for Nachmans method was presented by Siltanen, Mueller and Isaacsson in 2000. In 2006 Kari Astala and Lassi Päivärinta [18] proved uniqueness without any smoothness assumptions for the 2D case.

1.2 Some applications of EIT

Due to the fact that EIT equipment is relatively low cost and the technology to create mesurement devices already exists it has many applications in medical imaging and non-destructive testing.

In medical imaging it can provide a non-hazardous alternative to x-ray tomography which exposes the subject to radiation. However, EIT reconstruction methods are very sensitive to noise and do not detect small anomalies very well. Medical applications of EIT include monitoring lungs to detect a collapsed lung or fluid accumulation, detecting breast cancer, monitoring cardiac function or mechanical ventilation, detecting pulmonary embolus and pulmonary edema caused by high altitude.

In geophysics the imaging technique is often referred to as electrical resistivity tomography or electrical resistivity imaging. However, mathematically they deal with the same inverse problem and the theoretical study for both of these problems is the same. Applications of ERT include fault investigation, ground water table investigation and determining the content of soil mixture.

There are also many industrial applications e.g. in mining, pulp and paper industries. EIT can be used to detect air bubbles inside an object or to gain information on mixing processes.

Chapter 2

The Dirichlet-to-Neumann map

In this chapter our goal is to give the definition of a Dirichlet-to-Neumann map in EIT and to prove some basic results regarding the map. We begin by deriving the Dirichlet problem in EIT. This problem arises from the fundamentals of electromagnetism. Our approach in sections 2.1, 2.4 and 2.5 is similar to the approach in [1]. In sections 2.2.1 and 2.3 we follow the same structure as in [6].

2.1 Maxwell's equations

The mathematical model for electromagnetic fields can be obtained from a set of three-dimensional partial differential equations called Maxwell's equations.

Definition 2.1. Let $E(x,t)$ be the electric field, $J(x,t)$ the current density, $D(x,t)$ the electric displacement field, $\rho(x,t)$ the free electric charge density, $B(x,t)$ the magnetic flux and $H(x,t)$ the magnetic strenght for a point $x \in \mathbb{R}^3$. The Maxwell's equations in differential form are

$$\nabla \cdot D = \rho \quad \text{(Gauss's law)} \tag{2.2}$$

$$\nabla \cdot B = 0 \quad \text{(Gauss's law for magnetism)} \tag{2.3}$$

$$\nabla \times E = -\frac{\partial B}{\partial t} \quad \text{(Faraday's law of induction)} \tag{2.4}$$

$$\nabla \times H = J + \frac{\partial D}{\partial t} \quad \text{(Ampere's law).} \tag{2.5}$$

In addition, Ohm's law implies that

$$J = \sigma(x, \omega)E, \tag{2.6}$$

where $\sigma(x, \omega)$ is the conductivity. In EIT, the current applied on the surface results in a current density of the form $\mathrm{Re}(Je^{i\omega t})$, where ω is the angular frequency of the current. Now equations (2.4) and (2.5) become

$$\nabla \times E(x) = -\frac{\partial B(x)e^{i\omega t}}{\partial t} = -i\omega B(x) \tag{2.7}$$

and

$$\nabla \times H(x) = J(x) + i\omega D(x). \tag{2.8}$$

We assume that the magnetic permeability μ is very small and that the electric and magnetic response of the object is linear and isotropic. Now

$$\begin{aligned} D &= \epsilon(x, \omega)E \text{ and} \\ B &= \mu(x, \omega)H, \end{aligned}$$

where $\epsilon(x)$ is the electric permittivity, $\mu(x)$ the magnetic permeability.

Now E and B can be linearized about $\mu = 0$ to obtain

$$\begin{aligned} E(x, \omega; \mu) &= E(x, \omega; 0) + \partial_\mu E(x, \omega; 0)\mu + \frac{1}{2!}\partial_\mu^2 E(x, \omega; 0)\mu^2 + \dots \\ &= E_0 + \mu E_1 + \mu^2 E_2 + \dots \text{ and} \\ B(x, \omega; \mu) &= B_0 + \mu B_1 + \mu^2 B_2 + \dots . \end{aligned}$$

Now using the approximation $\mu = 0$ equation (2.7) becomes

$$\nabla \times E_0(x, \omega) = -i\omega B_0(x, \omega),$$

and from the linear constitutive relation, it follows that $B_0(x, \omega) = 0$. Now

$$\nabla \times E_0 = 0.$$

The electric field E_0 can be expressed using the gradient of the electric potential u:

$$E_0 = -\nabla u.$$

Now from the linear constitutive relations, (2.8) and (2.6) we get the following equation

$$\nabla \times H = (\sigma + i\omega\epsilon)E.$$

Now we can take the divergence to get

$$\nabla \cdot (\nabla \times H) = \nabla \cdot ((\sigma + i\omega\epsilon)E).$$

Since the divergence of a curl is always zero we get

$$\nabla \cdot ((\sigma + i\omega\epsilon)E) = \nabla \cdot ((\sigma + i\omega\epsilon)\nabla u(x)) = 0.$$

This is the generalized Laplace equation which forms the basis of solving the inverse conductivity problem. In later studies we consider the 2D case with $\omega = 0$:

$$\nabla \cdot (\sigma \nabla u) = 0.$$

2.2 The Dirichlet problem in EIT

2.2.1 The Dirichlet problem

In EIT we want to solve the inverse conductivity problem i.e. determine the unknown conductivity distribution σ inside the domain Ω by using current and voltage measurements on the boundary. The direct problem is to determine the voltage-to-durrent-density map on the boundary with known conductivity distribution inside the object. In order to find the voltage-to-current-density map we must solve a partial differential equation to find out the voltage distribution inside the object. This is known as the *Dirichlet problem in EIT*. The problem is as follows:

Find such $u \in \Omega$, that satisfies

$$\nabla \cdot \sigma \nabla u = 0, \text{ in } \Omega, \text{ where } u|_{\partial\Omega} = f \tag{2.9}$$

Here $\Omega \subset \mathbb{R}^n$ is the reconstruction domain and $\partial\Omega$ the boundary of the domain. The condition $u|_{\partial\Omega} = f$ is known as the *Dirichlet boundary condition*.

2.2.2 Weak solutions

In practice the conductivity σ usually has discontinuities. Therefore the term $\nabla \cdot \sigma \nabla u$ cannot be treated using regular derivatives. To overcome this problem we introduce the concept of a *weak solution*.

First, we give the definition of a weak solution to a similar Dirichlet-problem. This will be a useful step in proving that the problem (2.9) has a unique weak solution. We begin by introducing a theorem that will prove to be useful in the future.

To distinguish the L^2 inner product from the cartesian inner product we will use the following notation for the L^2 inner product from now on:

$$(u, v) = \int_\Omega u\overline{v}\, dx, \tag{2.10}$$

for all $u, v \in L^2$.

Theorem 2.11. *Let $\sigma \in L^\infty(\Omega)$. Now if there is a positive constant M such that*

$$\frac{1}{M} \leq \sigma(x) \leq M, \text{ for almost all } x \in \Omega, \tag{2.12}$$

then the conjugate linear pairing

$$(u, v)_\sigma \mapsto (\nabla u, \sigma \nabla v)$$

defines an inner product $(\cdot, \cdot)_\sigma$ on the closed subspace $H_0^1(\Omega)$. Additionally, the pairing defines the norm $\|\cdot\|_\sigma$, which is determined by its equivalence with the H^1-norm.

Proof. Let $u \in C_0^\infty$. Now by the Poincaré inequality B.5 and the condition 2.12 we get the following equation

$$\|u\|^2_{H^1(\Omega)} = \|u\|^2_{L^2(\Omega)} + \|\nabla u\|^2_{L^2(\Omega)} \leq (C(\Omega)^2 + 1)M^2 \|u\|^2_\sigma.$$

Now also

$$\|\nabla u\|^2_\sigma \leq M^2 \|\nabla u\|^2 \leq \|u\|^2_{H^1(\Omega)}.$$

Therefore the norms are equivalent in C_0^∞ which proves the theorem. □

We use the following as motivation for our definition. Assume that σ is differentiable and there is a positive constant M such that

$$\frac{1}{M} \leq \sigma(x) \leq M, \text{ for almost all } x \in \Omega.$$

If $u \in C_0^2(\Omega)$ solves the equation

$$\nabla \cdot \sigma \nabla u = f,$$

where $f \in L^2(\Omega)$, then using integration by parts we get

$$(\nabla u, \sigma \nabla v) = (f, v), \text{ for all } v \in C_0^\infty(\Omega).$$

Using this as a motivation we get the following definition:

Definition 2.13. Assume that $f \in L^2(\Omega)$. Now a function $u \in H_0^1(\Omega)$ is called *a weak solution* of the following Dirichlet-problem

$$\nabla \cdot \sigma \nabla u = f, \quad u|_{\partial\Omega} = 0, \tag{2.14}$$

if

$$(\nabla u, \sigma \nabla v) = (f, v), \tag{2.15}$$

for all $v \in H_0^1(\Omega)$.

We can prove the existence and uniqueness of the weak solution to the Dirichlet-problem 2.15:

Theorem 2.16. *Assume that $f \in L^2(\Omega)$. The Dirichlet problem*

$$\nabla \cdot \sigma \nabla u = f, \quad u|_{\partial\Omega} = 0$$

has a unique weak solution $u \in H_0^1(\Omega)$.

Proof. Let $\lambda_f(v) = (f, v)$ for $v \in H_0^1(\Omega)$. This defines a bounded linear functional on $H_0^1(\Omega)$ for any $f \in L^2(\Omega)$. Now by the Riesz representation theorem A.2 there exists a unique $u \in H_0^1(\Omega)$ such that

$$(u, v_\sigma) = \lambda_f(v),$$

for all $v \in H_0^1$. Now using the conjugate linear pairing in (2.11) we get

$$(\nabla u, \sigma \nabla v) = (u, v_\sigma) = \lambda_f(v) = (f, v),$$

for all $v \in H_0^1$. □

2.2.3 Uniqueness and existence of the solution

Now we are ready to prove the solvability and uniqueness of the Dirichlet-problem in EIT 2.9. We can formulate the problem using the *trace map* introduced in B.8.

First, consider the following Dirichlet-problem: Let $f \in H^{1/2}(\partial\Omega)$. Find a function $u \in H^1(\Omega)$ such that

$$(u, v)_\sigma = 0, \text{ for all } v \in H_0^1(\Omega), \tag{2.17}$$

where $\mathrm{tr}(u) = f$.

Theorem 2.18. *Let $\sigma \in L^\infty(\Omega)$ and there is a positive constant M such that*

$$\frac{1}{M} \leq \sigma(x) \leq M, \text{ for almost all } x \in \Omega.$$

Now the problem 2.17 has a unique solution $u \in H^1(\Omega)$

Proof. We begin by proving the uniqueness of the solution. Assume that u solves the problem 2.17 with $f = 0$. Now by theorem B.9 we have $u \in H_0^1(\Omega)$. Since u is now a solution of the weak problem 2.15 with $f = 0$ by theorem 2.13 it is unique.

Next we prove the existence. Let $F = Ef \in H^1(\Omega)$ be the extension of f. Now we define the term $\nabla \cdot \sigma \nabla F$ to belong to the dual of $H_0^1(\Omega)$ by identifying it with the linear functional

$$\lambda(F) : \theta \mapsto -(\sigma \nabla \theta, \nabla F),$$

where $\theta \in H_0^1(\Omega)$. Now the functional λ depends linearly on F.

Now by the Riesz-representation theorem A.2 there is a unique $U \in H_0^1(\Omega)$ satisfying the following equation

$$(\theta, U)_\sigma = \lambda(F)(\theta)$$

for all $\theta \in H_0^1(\Omega)$. Now the function $u = U + F$ is a weak solution to 2.17. □

2.2.4 Example of a solution

The Dirichlet problem can be solved analytically in some simple cases where the conductivity σ is rotationally symmetric. We will provide an example of such case but first we will prove a useful theorem regarding the Laplace operator.

Theorem 2.19. *Let $x = r\cos\theta$ and $y = r\sin\theta$, where $r \geq 0$ and $\theta \in [0, 2\pi]$. Now the Laplace operator Δ can be transformed to polar coordinates with the following identity*

$$\Delta v(x, y) = \frac{1}{r}\frac{\partial v(r,\theta)}{\partial r} + \frac{1}{r^2}\frac{\partial^2 v(r,\theta)}{\partial \theta^2} + \frac{\partial^2 v(r,\theta)}{\partial r^2},$$

where $v : \mathbb{R}^2 \to \mathbb{R}$.

Proof. Using the chain rule we get

$$\begin{aligned}
\frac{\partial v}{\partial r} &= \cos\theta \frac{\partial v}{\partial x} + \sin\theta \frac{\partial v}{\partial y} \\
\frac{\partial v}{\partial \theta} &= -r\sin\theta \frac{\partial v}{\partial x} + r\cos\theta \frac{\partial v}{\partial y}.
\end{aligned}$$

Differentiating a second time we get

$$\frac{\partial^2 v}{\partial r^2} = \cos^2\theta \frac{\partial^2 v}{\partial x^2} + \sin^2\theta \frac{\partial^2 v}{\partial y^2}$$
$$\frac{\partial^2 v}{\partial \theta^2} = r^2 \sin^2\theta \frac{\partial^2 v}{\partial x^2} - r\cos\theta \frac{\partial v}{\partial x} + r^2 \cos^2\theta \frac{\partial^2 v}{\partial y^2} - r\sin\theta \frac{\partial v}{\partial y}.$$

Now using these results we get the identity

$$\begin{aligned}\frac{1}{r}\frac{\partial v}{\partial r} + \frac{1}{r^2}\frac{\partial^2 v}{\partial \theta^2} + \frac{\partial^2 v}{\partial r^2} &= \frac{1}{r}\cos\theta \frac{\partial v}{\partial x} + \sin\theta \frac{\partial v}{\partial y} + \cos^2\theta \frac{\partial^2 v}{\partial x^2} + \sin^2\theta \frac{\partial^2 v}{\partial y^2} \\ &\quad + \frac{1}{r^2}\left(r^2 \sin^2\theta \frac{\partial^2 v}{\partial x^2} - r\cos\theta \frac{\partial v}{\partial x} + r^2\cos^2\theta \frac{\partial^2 v}{\partial y^2} - r\sin\theta \frac{\partial v}{\partial y}\right) \\ &= (\sin^2\theta + \cos^2\theta)\frac{\partial^2 v}{\partial x^2} + (\sin^2\theta + \cos^2\theta)\frac{\partial^2 v}{\partial y^2} \\ &= \frac{\partial^2 v}{\partial x^2} + \frac{\partial^2 v}{\partial y^2} = \Delta v.\end{aligned}$$

□

Now consider the following case with a single cocentric rotationally symmetric anomaly.

Example 2.20. Let $\Omega \subset \mathbb{R}^2$ be the unit disk and $\partial\Omega$ its boundary. Now we must solve the conductivity equation

$$\nabla \cdot \sigma \nabla u = 0, \text{ in } \Omega, \quad u|_{\partial\Omega} = f.$$

In order to define a cocentric anomaly we use polar coordinates denoted by r, θ. Now let us consider the following conductivity distribution

$$\sigma_{C,\rho}(r,\theta) := \begin{cases} 1 + C & , 0 \le r < \rho \\ 1 & , \rho \le r \le 1, \end{cases}$$

where $C > 0$ and $\rho \in (0,1)$. We choose the voltage on the boundary to be $f_n(\theta) := e^{in\theta}$ for some $n \in \mathbb{Z}$. There are apparent reasons for choosing this voltage distribution.

For solving the problem we use a technique called separation of variables. In order to use it, we assume that the solution can be separated into its radial and angular components i.e. $u(r,\theta) = R(r)\Theta(\theta)$. Now the boundary condition can be written as follows

$$R(1)\Theta(\theta) = f_n(\theta) = e^{in\theta}.$$

Therefore

$$R(1) = 1 \text{ and } \Theta(\theta) := e^{in\theta}.$$

Now let $R := R_1$ for $r < \rho$ and $R := R_2$ for $r > \rho$. Since $\sigma_{C,\rho}$ is now constant in both cases, we get

$$\sigma_{C,\rho}\Delta u = 0, \text{ for } 0 < r < \rho \text{ or } \rho < r < 1. \tag{2.21}$$

The Laplace operator Δ in polar coordinates is determined as

$$\Delta u = \frac{1}{r}u_r + u_{rr} + \frac{1}{r^2}u_{\theta\theta} = \frac{1}{r}R'\Theta + R''\Theta + \frac{1}{r^2}R\Theta''.$$

Now we can differentiate $\Theta(\theta) = e^{in\theta}$ twice to get $\Theta''(\theta) = -n^2e^{in\theta} = -n^2\Theta(\theta)$. Therefore

$$\Delta u = \frac{1}{r}R'\Theta + R''\Theta + \frac{1}{r^2}R\cdot(-n^2\Theta) = \Big(\frac{1}{r}R' + R'' + \frac{-n^2}{r^2}R\Big)\Theta.$$

Now since $\Theta \neq 0$ the equation (2.21) becomes the following:

$$\sigma_{C,\rho}(r^2R'' + rR' - n^2R) = 0.$$

Since $\sigma_{C,\rho} > 0$ we get the following ordinary differential equations:

$$\begin{aligned} r^2R_1'' + rR_1' - n^2R_1 = 0, &\quad 0 < r < \rho \\ r^2R_2'' + rR_2' - n^2R_2 = 0, &\quad \rho < r < 1. \end{aligned}$$

These are Euler equations which have the following solutions:

$$\begin{aligned} R_1(r) = C_1r^{|n|} + C_2r^{-|n|}, &\quad 0 < r < \rho \\ R_2(r) = C_3r^{|n|} + C_4r^{-|n|}, &\quad \rho < r < 1, \end{aligned}$$

where $n \neq 0$ and C_1, C_2, C_3 and C_4 are constants.

The next step is to determine the constants C_i by using boundary conditions. Since we do not have a boundary condition at $r = 0$, we can impose a condition that u is bounded near $r = 0$, i.e. $|R_1(0)| < \infty$. Therefore

$$C_2 = 0.$$

Since $R_2(1) = 1$, we know that

$$1 = R_2(1) = C_3 \cdot 1^{|n|} + C_4 \cdot 1^{-|n|} = C_3 + C_4.$$

For our solution we also need to have u and $\sigma_{C,\rho}\frac{\partial}{\partial r}u$ continuous at $r = \rho$. This implies that

$$\begin{aligned} &R_2(\rho) = R_1(\rho) \text{ and} \\ &R_2'(\rho) = (1 + C)R_1'(\rho). \end{aligned} \tag{2.22}$$

This implies that

$$\begin{aligned} & C_3\rho^{|n|} + C_4\rho^{-|n|} = C_1\rho^{|n|} \\ \Leftrightarrow \quad & C_3 - C_1 + C_4\rho^{-2|n|} = 0. \end{aligned}$$

Also from (2.22) we get

$$\begin{aligned} & |n|C_3\rho^{|n|} + C_4\rho^{-|n|} = C_1\rho^{|n|} \\ \Leftrightarrow \quad & (1+C)C_1 - C_3 + C_4\rho^{-2|n|} = 0. \end{aligned}$$

Now we have the following linear system of three equations with three unknowns:

$$\begin{aligned} C_3 + C_4 &= 1, \\ C_3 - C_1 + C_4\rho^{-2|n|} &= 0 \text{ and} \\ (1+C)C_1 - C_3 + C_4\rho^{-2|n|} &= 0. \end{aligned}$$

By solving the system we acquire the constants

$$C_1 = \frac{2}{k_n}, \quad C_2 = \frac{2+C}{k_n}, \quad C_3 = \frac{-C\rho^{2|n|}}{k_n}$$

Now since $u = R\Theta$, the solution to the Dirichlet problem is

$$u_n(r,\theta) = \begin{cases} \dfrac{2r^{|n|}}{2 + C(1-\rho^{2|n|})} e^{in\theta}, & 0 < r < \rho \\ \dfrac{(2+C)r^{|n|} - C\rho^{2|n|}r^{-|n|}}{2 + C(1-\rho^{2|n|})} e^{in\theta}, & \rho < r < 1, \end{cases}$$

where $n \in \mathbb{Z}$.

2.3 The Dirichlet-to-Neumann map

In this section our goal is to define a map which takes the given voltage distribution to the current-density distribution on the boundary. This map is called *Dirichlet-to-Neumann map* or the voltage-to-current-density map. Our approach is similar to the approach in [6] and many of the proofs and additional information can be found there.

Let $\Omega \subset \mathbb{R}^2$. Now the voltage distribution on the boundary f corresponds to the Dirichlet boundary condition

$$u|_{\partial\Omega} = f|_{\partial\Omega}$$

and the current density distribution J on the boundary is

$$J|_{\partial\Omega} = \sigma \frac{\partial u}{\partial \nu}\Big|_{\partial\Omega},$$

where ν is the outward pointing unit vector.

To give the definition of a Dirichlet-to-Neumann map we need to define a normal derivative for a function u which is a solution to the problem 2.17.

First, assume that everything is smooth. Now by Green's theorem we get the following equation

$$\int_{\partial\Omega} \sigma \frac{\partial u}{\partial \nu} h dS = \int_{\Omega} (\nabla \cdot \sigma \nabla u) v + \langle \nabla u, \nabla v \rangle dx,$$

where $v|_{\partial\Omega} = h$. Now when $\nabla \cdot \sigma \nabla u = 0$ in Ω we get

$$\int_{\partial\Omega} \sigma \frac{\partial u}{\partial \nu} h dS = \int_{\Omega} \sigma \langle \nabla u, \nabla v \rangle dx.$$

Now using the Trace-theorem we get the following estimate

$$\left| \int_{\Omega} \sigma(\nabla u, \nabla v) dx \right| \leq C \|u\|_{H^1(\Omega)} \|v\|_{H^1(\Omega)} \leq C_1 \|f\|_{H^{1/2}(\partial\Omega)} \|h\|_{H^{1/2}(\partial\Omega)}.$$

Therefore the bilinear form

$$(f, h) \mapsto \int_{\partial\Omega} \sigma \frac{\partial u}{\partial \nu} h dS$$

where u is a solution of the problem 2.17 defines a bounded linear functional on $H^{1/2}(\partial\Omega)$. We call this element the *normal derivative* of u.

Now we are ready to give the definition of the Dirichlet-to-Neumann map.

Definition 2.23. Let $u \in H^1$ be the unique solution to the Dirichlet problem (2.17). Now the map

$$\Lambda_\sigma : H^{1/2}(\partial\Omega) \to H^{-1/2}(\partial\Omega), \qquad \Lambda_\sigma : u|_{\partial\Omega} \longrightarrow \sigma \frac{\partial u}{\partial \nu}\Big|_{\partial\Omega}, \tag{2.24}$$

where Λ_σ is a bounded linear map, is the voltage-to-current-density or Dirichlet-to-Neumann map determined by the conductivity σ.

The DN map also has the following weak definition which we will use in the future.

Definition 2.25. Let $u \in H^1(\Omega)$ be the unique solution to the problem 2.17. Now the Dirichlet-to-Neumann map has the weak definition

$$\Lambda_\sigma : H^{1/2}(\partial\Omega) \to H^{-1/2}(\partial\Omega), \qquad (\Lambda_\sigma f, h)_{\partial\Omega} = \int_{\Omega} \sigma \langle \nabla u, \nabla v \rangle$$

where $v \in H^1(\Omega)$ is any function with trace h on the boundary.

2.4 The Neumann-to-Dirichlet map

In EIT we can either apply voltages on the boundary and measure current densities or apply a current and measure the voltage on the boundary. With this in mind we can define a map which takes current density on the boundary to voltage on the boundary. This map is called the *Neumann-to-Dirichlet map*.

In order to do this we must define the Neumann problem. The problem is as follows: Find such $u \in \Omega$, that satisfies

$$\nabla \cdot \sigma \nabla u = 0, \text{ in } \Omega, \qquad \text{where } \sigma \frac{\partial u}{\partial \nu}\bigg|_{\partial\Omega} = g$$

and $\int_{\partial\Omega} g \, dS = 0$.

Definition 2.26. Let $u \in H^1$ be the unique solution to the Neumann problem. The map

$$\mathcal{R}_\sigma g = u|_{\partial\Omega}$$

is called the Neumann-to-Dirichlet map.

Next, we introduce two theorems regarding the boundedness and other properties of the map. The proofs of these theorems follow from the standard theory of elliptic partial differential equations. A thorough study can be found in [4]. However, since the Neumann data implies the condition $\int_{\partial\Omega} g \, dS = 0$ we must first introduce a new function space $\widetilde{H}^s$.

Definition 2.27. Let $f \in H^s(\partial\Omega)$. Now $f \in \widetilde{H}^s$ if it satisfies the following conditions:

(i) $\dfrac{1}{|\partial\Omega|} \displaystyle\int_{\partial\Omega} f \, dS = 0$ and

(ii) $(f, c) = 0$ for all constant functions c,

i.e. $\widetilde{H}^s$ consists of H^s functions that are orthogonal to all constant functions and have mean value zero.

Theorem 2.28. *The Neumann-to-Dirichlet map*

$$\mathcal{R}_\sigma : \widetilde{H}^{-1/2}(\partial\Omega) \to H^{1/2}(\partial\Omega)$$

is bounded.

Theorem 2.29. *The Neumann-to-Dirichlet map $\mathcal{R}_\sigma$ is self-adjoint, smoothing and compact.*

Now we can see two key equalities concerning Λ_σ and $\mathcal{R}_\sigma$. First, define a projection operator

$$P\Lambda_\sigma := |\partial\Omega|^{-1} \int_{\partial\Omega} \phi \, dS.$$

Now for any $f \in H^{1/2}(\partial\Omega)$ we have

$$P\Lambda_\sigma f = |\partial\Omega|^{-1} \int_{\partial\Omega} \sigma \frac{\partial u}{\partial v} \, dS = |\partial\Omega|^{-1} \int_\Omega \nabla \cdot \sigma \nabla u \, dz = 0,$$

and therefore $\Lambda_\sigma : H^{1/2}(\partial\Omega) \to \widetilde{H}^{-1/2}(\partial\Omega)$. Now from the definitions of Λ_σ and $\mathcal{R}_\sigma$ we get the following equalities:

$$\begin{array}{lll} \Lambda_\sigma \mathcal{R}_\sigma & = I & : \widetilde{H}^{-1/2}(\partial\Omega) \to \widetilde{H}^{-1/2}(\partial\Omega) \\ \mathcal{R}_\sigma \Lambda_\sigma & = I - P & : H^{1/2}(\partial\Omega) \to \widetilde{H}^{1/2}(\partial\Omega) \end{array} \tag{2.30}$$

2.5 Eigenfunctions and eigenvalues of the DN map

In this study we only consider the domain to be the unit circe i.e. $\Omega = \{x \in \mathbb{R}^2 \mid |x| \leq 1\}$. When the conductivity $\sigma(x)$ is rotationally symmetric we know the eigenfunctions and eigenvalues of the DN map. We begin by looking at our previous example 2.20 and deriving the eigenfunctions and eigenvalues of the DN map in this case.

Example 2.31. Let us consider the same conductivity distribution as in example 2.20. We have shown that the solution to the dirichlet problem is

$$u_n(r,\theta) = \begin{cases} \dfrac{2r^{|n|}}{2 + C(1-\rho^{2|n|})} e^{in\theta}, & 0 < r < \rho \\ \dfrac{(2+C)r^{|n|} - C\rho^{2|n|} r^{-|n|}}{2 + C(1-\rho^{2|n|})} e^{in\theta}, & \rho < r < 1, \end{cases}$$

Now the Dirichlet-to-Neumann map is

$$\begin{aligned} \Lambda_{\sigma_{C,\rho}} f_n = \frac{\partial}{\partial r} u_n|_{r=1} &= \frac{\partial}{\partial r} \left(\frac{(2+C)r^{|n|} - C\rho^{2|n|} r^{-|n|}}{2 + C(1-\rho^{2|n|})} e^{in\theta} \right) \Bigg|_{r=1} \\ &= \left(\frac{(2+C)|n| r^{|n|-1} + C\rho^{2|n|}|n| r^{-|n|-1}}{2 + C(1-\rho^{2|n|})} e^{in\theta} \right) \Bigg|_{r=1} \\ &= \frac{2 + C(1+\rho^{2|n|})}{2 + C(1-\rho^{2|n|})} |n| f_n \end{aligned}$$

Now we can see that functions $e^{in\theta}$, where $n \in \mathbb{Z}$ are the eigenfunctions of $\Lambda_{\sigma_{C,\rho}}$ and the corresponding eigenvalues are

$$\lambda_n = \frac{2 + C(1 + \rho^{2|n|})}{2 + C(1 - \rho^{2|n|})}|n|,$$

where $n \in \mathbb{Z}$.

Now we have shown that we can determine the eigenfunctions and eigenvalues of the DN map with a piecewise constant conductivity distribution with a single rotationally symmetric anomaly. We can also determine the eigenfunctions and eigenvalues for any piecewise constant and rotationally symmetric conductivity distribution by the following theorems.

Theorem 2.32. *Let $\Omega = \{x \in \mathbb{R}^2 \mid |x| \leq 1\}$. Consider the rotationally symmetric case $\sigma(x) = \sigma(|x|)$. Then the eigenfunctions ϕ_n of the DN map are Fourier basis functions*

$$\phi_n = (2\pi)^{-\frac{1}{2}} e^{in\theta}. \tag{2.33}$$

Proof. The proof is similar to the example 2.31. A more detailed approach can be found in [9]. □

Theorem 2.34. *Let $\Omega = \{x \in \mathbb{R}^2 \mid |x| \leq 1\}$ and $0 = r_0 < r_1 < \cdots < r_{N-1} < r_N = 1$, where $N \geq 2$. For $j = 1, \ldots, N$, let σ_j be positive real numbers such that $\sigma_j \neq \sigma_{j+1}$ and $\sigma_N = 1$. Define $\sigma(r) = \sigma_j$ for $r_{j-1} < r < r_j$, $j = 1, \ldots, N$. The eigenvalues of Λ_σ are*

$$\lambda_n = |n| - 2|n|(1 + C_{N-1})^{-1}, \tag{2.35}$$

where the numbers C_j are given recursively by $C_1 = \rho_1 r_1^{-2|n|}$ and

$$C_j = \frac{\rho_j C_{j-1} + r_j^{-2|n|}}{\rho_j + C_{j-1} r_j^{2|n|}}$$

for $j = 2, \ldots, N-1$, where

$$\rho_j = \frac{\sigma_{j+1} + \sigma_j}{\sigma_{j+1} - \sigma_j}.$$

Proof. Since $\lambda_0 = 0$, we only take the values $n \neq 0$. We will construct an H^1 function u_n which solves the equation $\nabla \cdot \sigma \nabla u_n = 0$ in Ω, with the boundary condition $u_n|_{r=1} = \phi_n$. Denote

$$u_n = v_n(r)e^{in\theta} \quad \text{and} \quad v_n(r) = a_j r^{|n|} + b_j r^{-|n|},$$

for $r_{j-1} \leq r < r_j$ where $j = 1, \ldots, N$. Now we set $b_1 = 0$ so that u_n is harmonic in the innermost disc.

Next, we match the limits on each radius by setting

$$v_n(r_j^-) = v_n(r_j^+) \quad \text{and} \quad \frac{\sigma_j \partial v_n(r_j^-)}{\partial r} = \frac{\sigma_{j+1} \partial v_n(r_j^+)}{\partial r}.$$

This results in the equation

$$a_j = \frac{\left(\frac{\sigma_j + \sigma_{j-1}}{\sigma_j - \sigma_{j-1}}\right) C_{j-2} + r_{j-1}^{-2|n|}}{\left(\frac{\sigma_j + \sigma_{j-1}}{\sigma_j - \sigma_{j-1}}\right) + C_{j-2} r_{j-1}^{2|n|}} b_j = C_{j-1} b_j$$

for $j = 2, \ldots, N$.

Now from the boundary condition $u_n|_{r=1} = \phi_n$ we get

$$(2\pi)^{-\frac{1}{2}} e^{in\theta} = u_n|_{r=1} = (a_N \cdot 1^{|n|} + b_N \cdot 1^{-|n|}) e^{in\theta}.$$

Therefore $a_N + b_N = (2\pi)^{-\frac{1}{2}}$.

It can be checked using Green's theorem that our function u_n is in H^1 and satisfies $\nabla \cdot \sigma \nabla u_n = 0$ in the weak sense. Now the current density on the boundary becomes

$$\begin{aligned} \frac{\partial u_n}{\partial r}|_{r=1} &= \frac{\partial}{\partial r}(a_N r^{|n|} + b_N r^{-|n|}) \phi_n|_{r=1} \\ &= (a_N |n| r^{|n|-1} - |n| b_N r^{-|n|-1}) \phi_n|_{r=1} \\ &= |n|(a_N - b_N) \phi_n. \end{aligned}$$

Therefore $\lambda_n = |n|(1 - b_N)$ and $b_N = \dfrac{1}{1 + C_{N-1}}$. This proves the theorem. □

The theorem above only provides us with the eigenvalues for conductivity distributions with at least one anomaly. However, we also need the eigenvalues for the constant conductivity $\sigma \equiv 1$. We use the notation Λ_1 for the DN map with this conductivity.

Theorem 2.36. *Let Λ_1 be the DN map with the conductivity distribution $\sigma \equiv 1$ and $\phi_n = (2\pi)^{-\frac{1}{2}} e^{in\theta}$. Now*

$$\Lambda_1 \phi_n = |n| \phi_n, \quad \textit{for all } n \in \mathbb{Z},$$

i.e. the n:th eigenvalue of the operator Λ_1 is $|n|$.

Proof. We can clearly see that $\Lambda_1\phi_0 = 0$. Therefore ϕ_0 is the eigenfunction with the corresponding eigenvalue 0. Next we consider the case $n \in \mathbb{Z}\backslash\{0\}$. Now

$$\Delta z^n = \frac{\partial^2 z^n}{\partial x^2} + \frac{\partial^2 z^n}{\partial y^2} = n\frac{\partial z^{n-1}}{\partial x} + in\frac{\partial z^{n-1}}{\partial y} = n(n-1)z^{n-2}(1-1) = 0.$$

Next, we move to polar coordinates by setting $z^n = r^{|n|}e^{in\theta}$. Now $z^n|_{\partial\Omega} = e^{in\theta} = \sqrt{2\pi}\phi_n$. Let $\hat{r}$ and $\hat{\theta}$ be the basis vectors for the polar coordinates. Now the outward-pointing normal on the boundary is $\nu = \hat{r}$. Finally, by differentiating we get

$$\begin{aligned}
\Lambda_1\phi_n &= \frac{\partial\phi_n}{\partial\nu} \\
&= \left(\hat{r}\frac{\partial\phi_n}{\partial r} + \hat{\theta}\frac{1}{r}\frac{\partial\phi_n}{\partial\theta}\right)\cdot\nu \\
&= \frac{1}{\sqrt{2\pi}}\left(\hat{r}\frac{\partial r^{|n|}e^{in\theta}}{\partial r} + \hat{\theta}\frac{1}{r}\frac{\partial r^{|n|}e^{in\theta}}{\partial\theta}\right)\cdot\hat{r}\Bigg|_{r=1} \\
&= \frac{1}{\sqrt{2\pi}}\frac{\partial r^{|n|}e^{in\theta}}{\partial r}\Bigg|_{r=1} \\
&= \frac{1}{\sqrt{2\pi}}|n|r^{|n|-1}e^{in\theta}\Bigg|_{r=1} \\
&= \frac{1}{\sqrt{2\pi}}|n|e^{in\theta} \\
&= |n|\phi_n.
\end{aligned}$$

□

Note that the eigenvalues in the case of one or more anomalies are of the form $\lambda_n = |n| + \epsilon$, where ϵ is exponentially small as shown in [12]. Therefore, it is very difficult to accurately compute the eigenvalues with large values of n. However, we can compute the difference $\Lambda_\sigma - \Lambda_1$. Now since the n:th eigenvalue of Λ_1 is $|n|$, the n:th eigenvalue of $\Lambda_\sigma - \Lambda_1$ is precisely $2|n|(1 + C_{N-1})^{-1}$. Now we can use the difference to compute DN maps with very high accuracy when testing EIT algorithms with low noise level.

Chapter 3

The Dirichlet-to-Neumann matrix

In this chapter we introduce the Dirichlet-to-Neumann matrix (DN matrix) which is an approximation of the DN map. The matrix can be computed using the methods explained in section 3.1. We will restrict ourselves to $\Omega \subset \mathbb{R}^2$ being the unit disk since our computations are done using this set.

Our goal in this study is to analyze the DN matrix using Principal component analysis explained in 3.2. More information on the Finite element method can be found in [3] and [1]. An introduction and additional information on Principal component analysis can be found in [10].

3.1 Computing the DN matrix

3.1.1 Matrix approximation of a bounded linear operator

Let $\mathcal{A}$ be a bounded linear operator $\mathcal{A} : H^s(\partial\Omega) \to H^r(\partial\Omega)$. We can construct a matrix approximation to $\mathcal{A}$ using Fourier series. Denote $f \in H^s(\partial\Omega)$ and $g = \mathcal{A}f \in H^r(\partial\Omega)$. If the Fourier series of f and g have correct convergence properties, then

$$g(\theta) = \mathcal{A}f(\theta) = \mathcal{A} \sum_{n=-\infty}^{\infty} \hat{f}(n)\phi_n(\theta) = \sum_{n=-\infty}^{\infty} \hat{f}(n)\mathcal{A}\phi_n(\theta)$$

where $\phi_n = (2\pi)^{-\frac{1}{2}} e^{in\theta}$ are the Fourier basis functions. Now we can determine the function g by computing its Fourier coefficents

$$\hat{g}(m) := \langle \phi_m, g \rangle = \langle \phi_m, \sum_{n=-\infty}^{\infty} \hat{f}(n)\mathcal{A}\phi_n(z) \rangle = \sum_{n=-\infty}^{\infty} \hat{f}(n)\langle \phi_m, \mathcal{A}\phi_n(z) \rangle.$$

We can now approximate the functions f and g using the truncated sums

$$f(\theta) \approx \sum_{n=-N}^{N} \hat{f}(n)\phi_n(\theta) \text{ and } g(\theta) \approx \sum_{n=-N}^{N} \hat{g}(n)\phi_n(\theta),$$

where $N > 0$. Finally, we can construct a matrix approximation $A : \mathbb{C}^{2N+1} \to \mathbb{C}^{2N+1}$ of the operator $\mathcal{A}$ by defining the elements as follows:

$$A(m,n) := \langle \mathcal{A}\phi_n, \phi_m \rangle = \frac{1}{2\pi} \int_0^{2\pi} (\mathcal{A}e^{in\theta})e^{-im\theta} d\theta,$$

where we use the indexing $m \in \{-N, \ldots, N\}$ for the rows and $n \in \{-N, \ldots, N\}$ for the columns.

3.1.2 Computing the DN matrix using FEM

In our study we choose the unit disk $\Omega \subset \mathbb{R}^2$ as our domain. We will be using this domain from now on. We wish to construct a matrix approximation $\mathbf{L}_\sigma$ to our bounded linear operator

$$\Lambda_\sigma : H^{1/2}(\partial\Omega) \to H^{-1/2}(\partial\Omega).$$

We do this by using the method described in the previous section. Choose some $N > 0$ and choose the truncated basis from 2.33 with $-N \leq n \leq N$. Now we approximate the DN map by the $(2N+1) \times (2N+1)$ matrix $\mathbf{L}_\sigma = [(\mathbf{L}_\sigma)_{m,n}]$ defined by

$$(\mathbf{L}_\sigma)_{m,n} := (\Lambda_\sigma \phi_n, \phi_m) = \frac{1}{\sqrt{2\pi}} \int_0^{2\pi} (\Lambda_\sigma \phi_n) e^{-im\theta}\, d\theta. \tag{3.1}$$

Above we use the indexing $m \in [-N, \ldots, N]$ for the rows and $n \in [-N, \ldots, N]$ for the columns.

The matrix $\mathbf{L}_\sigma$ can be computed numerically using the Finite Element Method (FEM). The finite element method is used to compute an approximation of the solution to the Dirichlet problem. To use the method we must use the weak formulation of the Dirichlet problem. Consider the Dirichlet problem in 2.9. The weak formulation of the problem is as follows:

Find such $u \in H^1(\Omega)$ that

$$(\nabla u, \sigma \nabla v) = 0, \qquad u|_{\partial\Omega} = f, \tag{3.2}$$

for all $v \in H_0^1(\Omega)$. Again, we use the same notation for the L^2 inner product as described in 2.10.

The idea is to discretise the domain Ω into finite elements and define basis functions v_i which vanish on most of these elements. The finite elements used in our 2-dimensional case are triangles. These elements form a mesh that covers the domain Ω. An example of a very fine mesh can be found in figure 4.2.

The solution u is then approximated in a finite-dimensional function space using the basis functions v_i. These basis functions are usually not defined directly. Instead a function type, the so called ansatz function, (e.g. linear or quadratic polynomial) is selected which the approximation of u should adopt on each of these elements. A common choice is a linear ansatz function, which means that the approximation will be a linear function on each element and continuous over Ω but not continuously differentiable. This is the reason behind the weak formulation of the problem.

Each of the elements possess a set of distinguishing nodes and vertices. In our case the nodes are located at the center and at the corners of each tringle and are the degrees of freedom of the ansatz function.

This results in a finite system which is solved to give the approximation of u in the finite-dimensional function space defined by the basis functions v_i. The accuracy of the approximation is dependent on the mesh used. Therefore, a finer mesh results in a better approximation.

In our case we use MATLAB's PDE Toolbox for the FEM implementation. When computing an approximation for the DN map we need to differentiate the approximate solution to evaluate

$$\Lambda_\sigma \phi_n = \frac{\sigma(\partial u_n)}{\partial \nu}|_{\partial\Omega}$$

and then use a quadrature rule to give an approximation to the integral in 3.1 for all $-N \leq m \leq N$, which yields the n:th column of our matrix $\mathbf{L}_\sigma$. These computations will be made for all $-N \leq n \leq N$ to build each column of the matrix.

3.1.3 Computing the ND matrix

Now we can approximate the DN map numerically by computing a matrix approximation of the map. Computing the matrix requires solving the Dirichlet problem which is done using finite element method. However, when computing the DN matrix we come up with the task of numerical differentiation which is unstable. For this reason we first compute the matrix approximation for the Neumann-to-Dirichlet map and compute its inverse.

Consider the space $\widetilde{H}^{-1/2}$ as defined in 2.27 and the Neumann-to-Dirichlet map

$$\mathcal{R}_\sigma : \widetilde{H}^{-1/2}(\partial\Omega) \to H^{1/2}(\partial\Omega).$$

Our goal is to compute its matrix approximation $\mathbf{R}_\sigma$.

First, consider the Neumann problem

$$\nabla \cdot \sigma \nabla u_n = 0 \text{ in } \Omega, \text{ with } \sigma \frac{\partial u_n}{\partial \nu}\bigg|_{\partial\Omega} = \phi_n, \tag{3.3}$$

where the solution u_n is determined up to an additive constant. To make the solution unique we require the following condition

$$\int_{\partial\Omega} u_n \, dS = 0.$$

Since $\int_{\partial\Omega} \sigma \frac{\partial u_n}{\partial \nu} \, dS = 0$, the problem (3.3) is well-defined only when $n \neq 0$. Therefore, we define $\mathbf{R}_\sigma$ as a $2N \times 2N$ matrix with the basis $\phi_{-N}, \ldots, \phi_{-1}, \phi_1, \ldots \phi_N$ where we don't include the constant function $\phi_0 = (2\pi)^{-\frac{1}{2}}$.

When constructing the approximation our first step is to solve the Neumann problem (3.3) for

$$n = -N, \ldots, -1, 1, \ldots N$$

using the finite element method. We specify the Neumann data at the centers of the edge segments. When evaluating the trace $u_n|_{\partial\Omega}$ we simply choose the values of the solution u_n at the boundary nodes.

Now we set $\mathbf{R}_\sigma = [(\mathbf{R}_\sigma)_{\mathbf{m},\mathbf{n}}] = \hat{\mathbf{u}}_\mathbf{n}(\mathbf{m})$ with

$$\hat{u}_n(m) = \langle u_n|_{\partial\Omega}, \phi_m \rangle = \frac{1}{\sqrt{2\pi}} \int_0^{2\pi} u_n|_{\partial\Omega}(\theta) e^{-in\theta} \, d\theta,$$

where m is the row index and n the column index. The integration is implemented with with a quadrature using the lengths of the boundary segments as weights.

3.1.4 Computing the DN matrix from the ND matrix

We can use the ND matrix to compute the DN matrix quite easily. We do this by using the inverse $\mathbf{R}_\sigma^{-1}$. Since the potential $u_n \in H^1(\Omega)$ is the same in both the Dirichlet and Neumann problems the DN and ND maps are each others inverses as seen in 2.30.

First, let

$$\mathbf{L}'_\sigma := \mathbf{R}_\sigma^{-1}.$$

Now $\mathbf{L}'_\sigma$ is a $2N \times 2N$ matrix. However, the DN matrix is a $(2N+1) \times (2N+1)$ since it uses the truncated basis with $n = -N, \ldots, N$ and possesses appropriate mapping properties for constant basis functions at the boundary.

It can be easily seen that $u \equiv 1$ is the unique solution of the Dirichlet problem $\nabla \cdot \sigma \nabla u = 0$ in Ω with $u|_{\partial\Omega} = 1$. Therefore, the DN operator satisfies

$$\Lambda_\sigma 1 = 0. \tag{3.4}$$

This in fact holds for all constant functions C, since the unique solution to the conductivity equation with $u|_{\partial\Omega} = C$ is $u = C$. Also, since the net current through the boundary must be zero we get

$$\int_{\partial\Omega} \Lambda_\sigma f \, dS = 0 \quad \text{for all } f \in H^{1/2}(\partial\Omega). \tag{3.5}$$

This states that functions of the form $\Lambda_\sigma f$ have zero as the constant component.

Using the conditions 3.4 and 3.5 we get our matrix approximation $\mathbf{L}_\sigma$ by adding a zero row and a zero column in the middle of our matrix $\mathbf{L}'_\sigma$. This also results in $(2N+1) \times (2N+1)$ matrix which was our goal. More precisely, we divide the matrix into 4 $N \times N$ blocks named as follows:

$$\mathbf{L}'_\sigma = \left[\begin{array}{c|c} \mathbf{L}'_\sigma\{1,1\} & \mathbf{L}'_\sigma\{1,2\} \\ \hline \mathbf{L}'_\sigma\{2,1\} & \mathbf{L}'_\sigma\{2,2\} \end{array}\right]$$

and construct the matrix $\mathbf{L}_\sigma$ by adding a zero row and column in the middle as follows:

$$\mathbf{L}_\sigma = \begin{bmatrix} \mathbf{L}'_\sigma\{1,1\} & \underset{N\times 1}{\mathbf{0}} & \mathbf{L}'_\sigma\{1,2\} \\ \underset{1\times N}{\mathbf{0}} & \underset{1\times 1}{\mathbf{0}} & \underset{1\times N}{\mathbf{0}} \\ \mathbf{L}'_\sigma\{2,1\} & \underset{N\times 1}{\mathbf{0}} & \mathbf{L}'_\sigma\{2,2\} \end{bmatrix}.$$

The effect of the zero column is that multiplying the vector representing the coefficents of the constant function $u = 1$ expressed in the Fourier basis

$$\begin{bmatrix} \underset{1}{0} & \cdots & \underset{N}{0} & \underset{N+1}{1} & \underset{N+2}{0} & \cdots & \underset{2N+1}{0} \end{bmatrix}^T$$

by the matrix $\mathbf{L}_\sigma$ on the left gives the zero vector. This is the discrete counterpart of 3.4. The effect of the zero row is that for any vector $\mathbf{f} \in \mathbb{R}^{2N+1}$ the vector $\mathbf{L}_\sigma\mathbf{f}$ has the form

$$\begin{bmatrix} \underset{1}{\bullet} & \cdots & \underset{N}{\bullet} & \underset{N+1}{0} & \underset{N+2}{\bullet} & \cdots & \underset{2N+1}{\bullet} \end{bmatrix}^T$$

This leads to the coefficent of ϕ_0 being 0 and it is the discrete counterpart of 3.5.

3.2 Principal component analysis

The next step in this study is to analyze the DN matrices that correspond to different conductivity distributions. The main problem in this analysis is to find out the useful

information from this high-dimensional data. In order to do this, a dimensionality reduction method is needed. In this study a method called *principal component analysis* is used for the task.

Principal component analysis is a statistical method used for finding out the components from the n-dimensional data X which have the most variance. These components are called the *principal components* of X. The principal components are linearly uncorrelated and each have a corresponding *principal value*.

The first step in PCA is to form the datamatrix X where each row of the matrix contains a repetition of the experiment. In our case each row contains the DN matrix in row form. Each column of the matrix therefore contains the values of one element of the DN matrix. Since the DN matrices are $n \times n$ -matrices the datamatrix is an $m \times n^2$ -matrix, where m is the number of matrices computed with different conductivity distributions.

The next step is to subtract the mean of the data. This means computing the mean value for each of the dimensions and subtracting each element of the column by the corresponding mean value.

After subtracting the mean from the data we can compute the covariance matrix. Covariance between two vectors $x, y \in \mathbb{R}^n$, where $x = (x_1, x_2, \ldots, x_n)$ and $y = (y_1, y_2, \ldots, y_n)$ is

$$cov(x, y) = \frac{\sum_{i=1}^{n}(x_i - \overline{x})(y_i - \overline{y})}{n - 1},$$

where $\overline{x}$ and $\overline{y}$ are the mean values of the corresponding vectors. The covariance between n-dimensional data can be represented as a covariance matrix $C \in \mathbb{R}^{n \times n}$ which is constructed as follows

$$C_{i,j} = cov(X_i, X_j),$$

where X_k is the k:th column of the data matrix X representing the k:th dimension. Now since the column means have been subtracted from the data matrix X we can estimate the covariance matrix as the sample correlation matrix

$$Q = \frac{1}{n} X^T X.$$

The principal components are now the eigenvectors of the covariance matrix C and the principal values are the corresponding eigenvalues.

Computing the covariance matrix and its eigenvectors is computationally challenging. However, we can use a more efficient method for finding out the principal components. This method is known as *singular value decomposition*.

3.2.1 PCA using singular value decomposition

The singular value decomposition of an $n \times m$ -matrix X is

$$X = USV^T.$$

Here U is an $n \times n$ -matrix where the columns consist of orthogonal unit vectors of length n, called the *left singular vectors* of X, the $n \times n$ -matrix S is a diagonal matrix which consists of positive diagonal elements called the *singular values* of X and the matrix $V \in \mathbb{R}^{m \times m}$ contains orthogonal unit vectors of length m called the *right singular vectors* of X.

Now we can write the covariance matrix $C = X^T X$ using the singular value decompostion as follows

$$X^T X = (USV^T)^T USV^T = VSU^T USV^T = VS^2V^T.$$

Since the matrix V consists of orthogonal unit vectors and the matrix S is a diagonal matrix we can compare this with the eigenvalue decomposition of $X^T X$ and notice that the right singular vectors of X are the eigenvectors of $X^T X$ and the singular values of X are the square roots of the eigenvalues of $X^T X$. Therefore, the principal components are exactly the right singular vectors of X and the principal values are the squares of the singular values of X.

3.2.2 Dimensionality reduction

Since the principal components of the data matrix X are orthogonal and the first components represent the directions with the most variance we can approximate the data by using only the first principal components. Using only the first components we can represent the data using fewer dimensions which are selected to maximize the variance and minize the error in the reconstruction.

We can reduce the dimension by computing the score matrix $T = US$ by including only the first singular values, i.e. the truncated score matrix T_n is defined as follows

$$T_n = US_n,$$

where

$$\begin{cases} (S_n)_{i,j} = S_{i,j}, & \text{when } 1 \leq i, j \leq k \\ (S_n)_{i,j} = 0, & \text{when } k \leq i, j \leq n. \end{cases}$$

The reconstruction

$$X_n = T_n V^T$$

contains the linear combinations of the first n principal components i.e. each row x_i of the data matrix X is approximated with the linear combination

$$x_i = t_{i,1}p_1 + t_{i,2}p_2 + \cdots + t_{i,n}p_n,$$

where $t_{i,k}$ is the element of the score matrix corresponding to the i:th measurement and the k:th principal component vector p_k.

Since the elements of the score matrix form the coefficents of the linear combinations which form the data matrix, we can study these coefficents to see the effect of each principal component on the data.

Chapter 4

Computations and results

One of the goals in this study was to understand the behaviour of the DN matrix corresponding to different conductivity distributions. The computations were simplified by studying the case of piecewise-constant conductivities in the unit circle. Our goal is to compute the principal components and values of the data and analyze the behavior of the DN matrix using these values.

The DN matrices were computed by first computing the ND matrix and using the inversion technique in section 3.1.4. Computing the matrix included solving the Neumann problem using FEM. This was done using MATLAB's PDE toolbox. The resulting matrices form the data matrix used in PCA with each row consisting of a DN matrix.

4.1 The conductivity distributions and FEM

Consider the unit circle as our set Ω with the boundary $\partial\Omega$. The conductivity distributions used were piecewise-constant conductivities with four different anomalies in the unit circle. The background conductivity outside the anomalies is $\sigma \equiv 1$. The four anomalies consisted of four tiles as seen in picture 4.1.

Let σ_n, where $n = 1, 2, 3, 4$, be the conductivity for each anomaly. The conductivities used were chosen in the interval $[0.4, 1.6]$ with a step of 0.2. Overall, this resulted in 7 different conductivities for each tile and $4^7 = 2401$ different conductivity distributions. The number of trigonometric basis functions used was $N = 5$. This resulted in $2N + 1 \times 2N + 1 = 11 \times 11$ DN matrices. Therefore the resulting datamatrix is of size $2401 \times (11 \cdot 11) = 2401 \times 121$.

In addition, the DN matrix for the constant conductivity σ_1, where $\sigma \equiv 1$, was computed. Due to the reasons mentioned in 2.5 the matrices included in the data were of the

form

$$\Lambda_{\sigma_k} - \Lambda_{\sigma_1},$$

where $k = 1, \ldots, 2401$ represents the conductivity distribution used. Computing the data matrix took approximately 8 hours on a regular desktop computer with a quad-core processor.

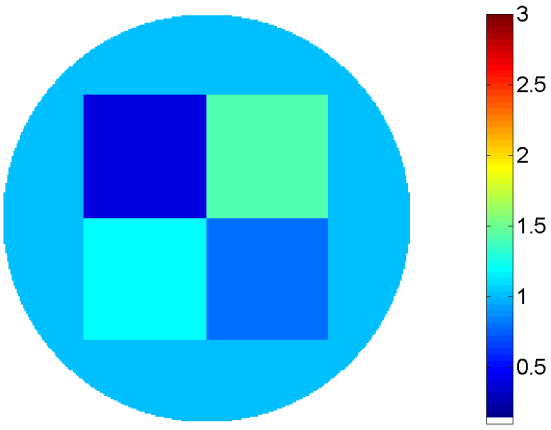

Figure 4.1: An example of a conductivity distribution used

The Neumann problem was solved using FEM as described in 3.1.2. The mesh was created using a premade Matlab routine and consisted of 65536 triangles and 33025 vertices. An image of the mesh used can be found in figure 4.2. In the image the vertices are shown in blue on a white background.

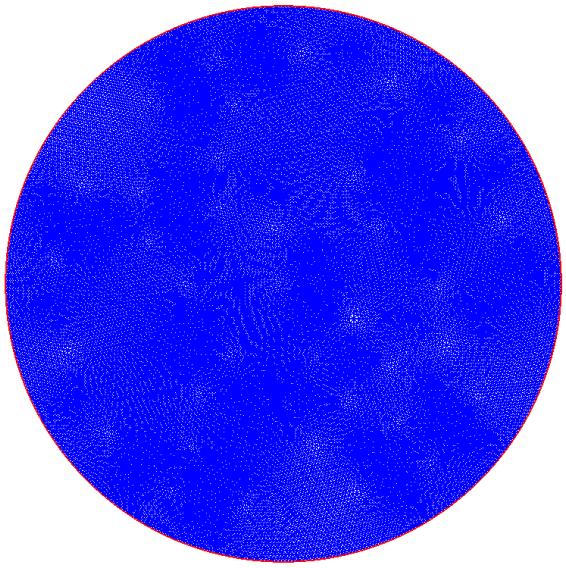

Figure 4.2: The mesh used in solving the Neumann problem with FEM

4.2 Principal components

The principal components of the DN matrix data were computed using SVD as described in 3.2. The singular value decomposition was done using Matlab's SVD routine. This resulted in three matrices: matrix U where the columns consist left singular vectors, a diagonal matrix with the singular values S and the matrix V containing the right singular vectors.

Now we get the principal components as the right singular vectors of the data matrix. Images of the first three principal components are shown in figures 4.3, 4.4 and 4.5. The matrices are shown as images rather than in the traditional form, since it is easier to visualize them this way.

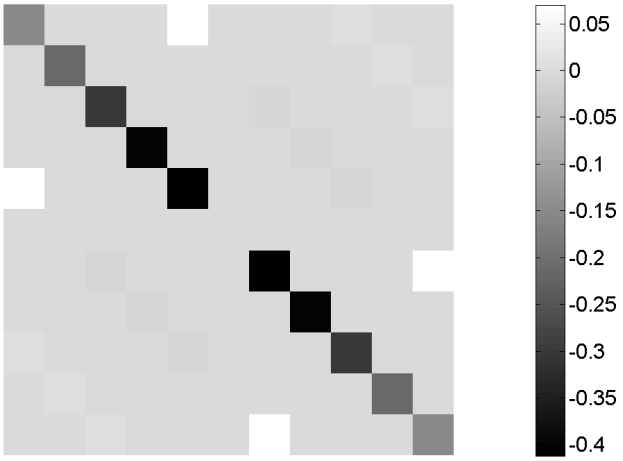

Figure 4.3: The first principal component

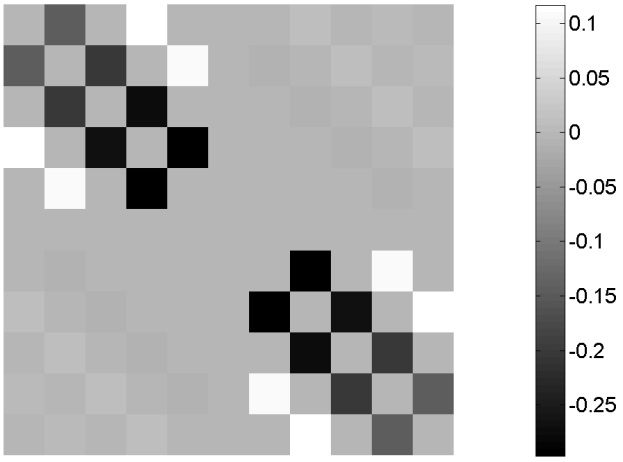

Figure 4.4: The second principal component

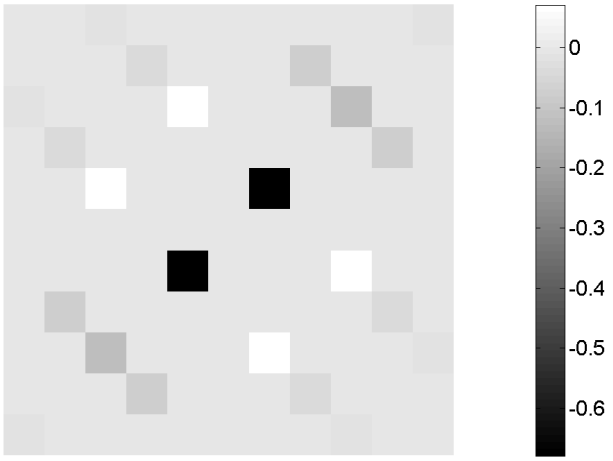

Figure 4.5: The third principal component

4.3 Principal values

All principal values were computed using the same approach. The singular values are obtained from the matrix S, which contains the values as its diagonal elements. Since the singular values are the square roots of the eigenvalues of the covariance matrix $C = X^T X$, we get the principal values as the squares of the singular values. The first 45 principal values can be found in table 4.3.

A logarithmic plot of first 40 principal values can be found in figure 4.6 and a logarithmic plot of all principal values can be found in figure 4.7.

Value no.	Value	Value no.	Value	Value no.	Value
1	134,4785177	16	$2,46935 \cdot 10^{-5}$	31	$1,04549 \cdot 10^{-25}$
2	92,18508562	17	$7,16807 \cdot 10^{-6}$	32	$7,30099 \cdot 10^{-26}$
3	0,719661564	18	$4,88032 \cdot 10^{-6}$	33	$6,5278 \cdot 10^{-26}$
4	0,351255821	19	$4,40929 \cdot 10^{-6}$	34	$4,39491 \cdot 10^{-26}$
5	0,319265082	20	$2,43369 \cdot 10^{-6}$	35	$3,9422 \cdot 10^{-26}$
6	0,166123473	21	$1,03723 \cdot 10^{-6}$	36	$2,88653 \cdot 10^{-26}$
7	0,114837613	22	$9,30906 \cdot 10^{-7}$	37	$2,51233 \cdot 10^{-26}$
8	0,056799296	23	$7,35296 \cdot 10^{-7}$	38	$2,45074 \cdot 10^{-26}$
9	0,001245244	24	$3,9394 \cdot 10^{-7}$	39	$1,91354 \cdot 10^{-26}$
10	0,001187612	25	$2,80313 \cdot 10^{-7}$	40	$1,57748 \cdot 10^{-26}$
11	0,000333355	26	$2,5065 \cdot 10^{-7}$	41	$1,44218 \cdot 10^{-26}$
12	0,000215312	27	$1,10792 \cdot 10^{-7}$	42	$1,25395 \cdot 10^{-26}$
13	$9,29489 \cdot 10^{-5}$	28	$3,8673 \cdot 10^{-8}$	43	$1,17798 \cdot 10^{-26}$
14	$7,53199 \cdot 10^{-5}$	29	$1,7231 \cdot 10^{-8}$	44	$1,06536 \cdot 10^{-26}$
15	$3,68571 \cdot 10^{-5}$	30	$2,61937 \cdot 10^{-9}$	45	$9,7068 \cdot 10^{-27}$

Table 4.1: The first 45 principal values

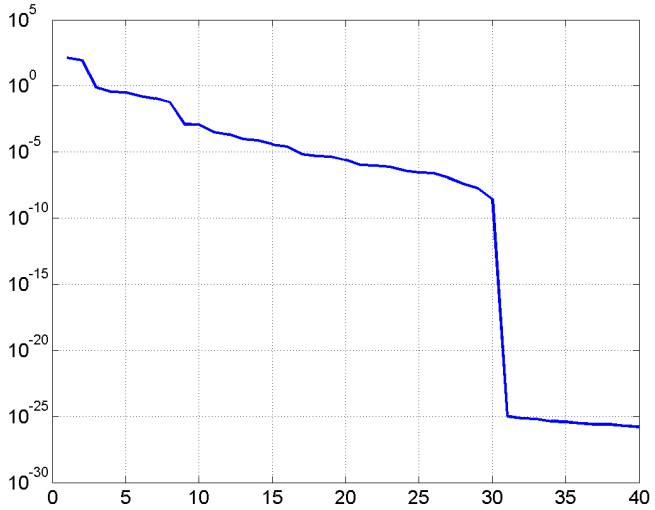

Figure 4.6: The first 40 principal values plotted on a logarithmic scale

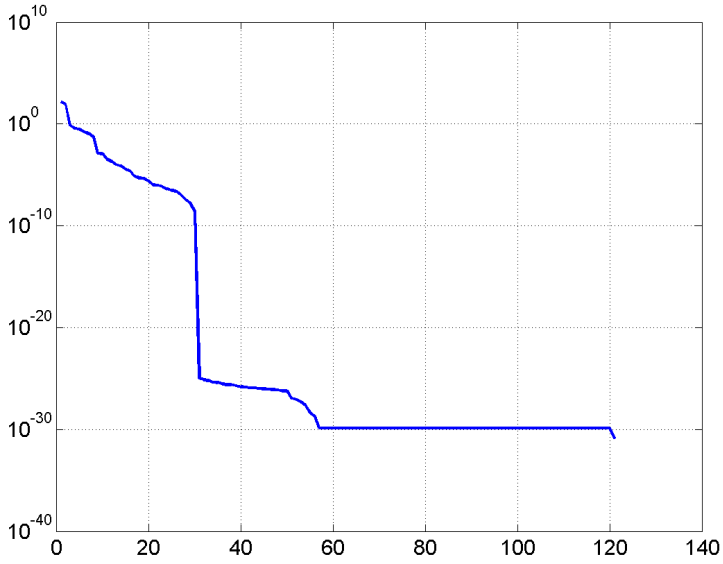

Figure 4.7: All principal values plotted on a logarithmic scale

4.4 Dimensionality reduction

The data was approximated using truncated score matrices described in 3.2. Approximations were made with $1, 2, 3, 10, 30, 40$ and all 121 singular values. The relative error for each $n \in \{1, 2, 3, 10, 30, 40, 121\}$ was computed as

$$E_n = \frac{\|\mathbf{R}_n - X\|_p}{\|X\|_p},$$

where $\mathbf{R}_n$ is the approximated data matrix using n singular values, as described in 3.2.2, and X is the data matrix.

The approximation made using all singular values was computed to form a baseline to see the computational error caused by the SVD routine. The relative errors for each approximation computed with the l^1, l^2 and l^∞ norms can be found in table 4.4.

No. of singular values	$l^1 - norm$	$l^2 - norm$	$l^\infty - norm$
1	0,905472113	0,827949551	0,591416237
2	0,093697578	0,073153936	0,095372668
3	0,092923199	0,051107579	0,057693884
10	0,003933957	0,001574443	0,000925099
30	$4,18211 \cdot 10^{-13}$	$2,78831 \cdot 10^{-14}$	$2,62817 \cdot 10^{-14}$
40	$5,53495 \cdot 10^{-14}$	$1,03634 \cdot 10^{-14}$	$9,10323 \cdot 10^{-15}$
121	$2,94284 \cdot 10^{-14}$	$2,74029 \cdot 10^{-15}$	$2,41259 \cdot 10^{-15}$

Table 4.2: The relative errors in different approximations

Chapter 5

Discussion

5.1 Principal values

One of the goals in this study was to find if the four variables in the conductivity distributions have some effect to the dimension of the hyperplane that the DN matrices form. Since our data is 121 dimensional it is impossible to visualize it using all of the data. Therefore PCA was used to reduce the dimension.

The principal values can be studied to determine which principal components have the biggest effect on the data. It can be clearly seen from the data in table 4.3 that the first two principal values are significantly greater than the rest. The third principal component is already two orders of magnitude smaller than the second one. Therefore the most of the variation in the DN matrices happens in the direction of these two components.

After the first two principal components we see a steady decrease in the values until the 30:th value. After the first 30 principal values there is another significant decrease. The 31:st principal value is 16 orders of magnitude smaller than the 30:th value. This can be seen clearly seen on the logarithmic plots 4.6 and 4.7.

5.2 Dimensionality reduction

The effect that each principal component has on the data can also be seen when computing an approximation of the data matrix using the truncated sums described in 3.2. We can clearly see from the relative errors shown in 4.4 that the error is already relatively small when using two components in the approximation. This corresponds to the fact that the first two principal values are much larger than the rest of the values.

We can also see that the error is almost insignificant when the approximation uses 30 singular values. The error in this case is very close to the error on the baseline

approximation using all 121 singular values. Therefore, the last 91 principal components have almost no effect on the data. Again, the result is in line with the significant decrease in the principal values.

These facts suggest that even with 4 degrees of freedom in the conductivity distribution the DN matrices vary primarily in a 2-dimensional subspace with the first two principal components as the directions of the most variation. We can also see that only 30 out of the 121 principal components have a notable effect on the data.

In this study we only computed the DN matrices for the special case of 4 anomalies in the unit circle. This case was already computationally quite demanding. With more time and more computational power the matrices could be computed for with different conductivity distributions to see if the principal components and values differ from these results.

Appendices

Appendix A

Functional analysis

In this chapter we present some of the basic concepts of functional analysis needed in our study. Our goal is to define the function spaces used and give some basic results of functional analysis and especially Fourier-analysis.

A.1 Some fundamental definitions and theorems in functional analysis

Our goal in this section is to introduce some basic definitions and theorems of functional analysis. We begin by giving the definition of dual space which will be used to define Sobolev spaces used in our study. We also introduce important theorems such as the *Riesz representation theorem* and *Green's formula*. More information on functional analysis can be found in [13], [6] and [14].

Definition A.1. Let H be a Hilbert space over a field F. The dual space H^* is the set of all linear maps

$$\phi : H \to F.$$

Theorem A.2. *Let X be a Hilbert space. Then for each bounded linear function $F : X \to \mathbb{C}$ there exists a unique element $f \in X$ such that*

$$F(\phi) = \langle \phi, f \rangle,$$

for all $\phi \in X$.

Next, we introduce three very useful theorems known as the *Divergence theorem*, *Green's first identity* and *Green's formula*. We begin with the Divergence theorem.

Theorem A.3. *Let $\Omega \in \mathbb{R}^n$, where $n \geq 2$, be a bounded domain with boundary $\partial\Omega$ and $\nu(x) = (\nu_1(x), \ldots, \nu_n(x))$ the outward-pointing unit normal at the boundary. Now*

$$\int_\Omega \nabla \cdot h(x)\, dx = \int_{\partial\Omega} \langle \nu(x), h(x) \rangle\, dS(x),$$

where $\langle \cdot, \cdot \rangle$ denotes the Euclidian inner product and $dS(x)$ is the surface measure on $\partial\Omega$.

Now assume that $f, g \in C^2(\Omega) \cap C^1(\overline{\Omega})$, where $\overline{\Omega}$ is the closure of Ω. Let $h = (\nabla f)g$. Now using the product rule of differentiation we get

$$\nabla \cdot h = (\Delta f)g + \langle \nabla f, \nabla g \rangle,$$

where $\Delta = \nabla \cdot \nabla$ is the Laplace operator. We also have

$$\langle \nu(x), (\nabla f)g \rangle = \langle \nu(x), \nabla f \rangle g = \frac{\partial f}{\partial \nu} g,$$

where $\dfrac{\partial f}{\partial \nu}$ is the normal derivative of f. Using these results we get Green's first identity.

Theorem A.4. *Let $\Omega \in \mathbb{R}^n$, where $n \geq 2$, be a bounded domain with boundary $\partial\Omega$. Now*

$$\int_\Omega (\Delta f)g + \langle \nabla f, \nabla g \rangle\, dx = \int_{\partial\Omega} \frac{\partial f}{\partial \nu} g\, dS(x).$$

Now we are ready to prove Green's theorem.

Theorem A.5. *Let $\Omega \in \mathbb{R}^n$, where $n \geq 2$, be a bounded domain with boundary $\partial\Omega$. Now*

$$\int_\Omega (\Delta f)g - f\Delta g\, dx = \int_{\partial\Omega} \frac{\partial f}{\partial \nu} g - f \frac{\partial g}{\partial \nu}\, dS(x).$$

Proof. By Green's first identity we get

$$\int_\Omega (\Delta f)g + \langle \nabla f, \nabla g \rangle\, dx = \int_{\partial\Omega} \frac{\partial f}{\partial \nu} g\, dS(x)$$

and

$$\int_\Omega f\Delta g + \langle \nabla f, \nabla g \rangle\, dx = \int_{\partial\Omega} f \frac{\partial g}{\partial \nu}\, dS(x).$$

Now by subtracting these equations we get

$$\begin{aligned}
&\int_\Omega (\Delta f)g + \langle \nabla f, \nabla g \rangle\, dx - \int_\Omega f\Delta g + \langle \nabla f, \nabla g \rangle\, dx = \int_{\partial\Omega} \frac{\partial f}{\partial \nu} g\, dS(x) - \int_{\partial\Omega} f \frac{\partial g}{\partial \nu}\, dS(x) \\
\Leftrightarrow \quad &\int_\Omega (\Delta f)g - f\Delta g + \langle \nabla f, \nabla g \rangle - \langle \nabla f, \nabla g \rangle\, dx = \int_{\partial\Omega} \frac{\partial f}{\partial \nu} g - f \frac{\partial g}{\partial \nu}\, dS(x) \\
\Leftrightarrow \quad &\int_\Omega (\Delta f)g - f\Delta g\, dx = \int_{\partial\Omega} \frac{\partial f}{\partial \nu} g - f \frac{\partial g}{\partial \nu}\, dS(x).
\end{aligned}$$

□

A.2 Fourier analysis

In this section our goal is to introduce the definitions of a *Fourier transform* and *Fourier series* and give some theorems that will be useful in our study. The proofs can be found in [2].

Definition A.6. Let $f : \mathbb{R}^n \to \mathbb{R}$. The *Fourier transform* of f is defined as

$$\mathcal{F}(x)(\xi) = \hat{f}(\xi) = \frac{1}{(2\pi)^n} \int_{\mathbb{R}^n} f(x) e^{-ix\xi} \, dx.$$

and the inverse Fourier transform is given by

$$\mathcal{F}^{-1}(f)(x) = \int_{\mathbb{R}} \hat{f}(\xi) e^{i\xi x} \, d\xi.$$

Definition A.7. Let $f : \mathbb{R} \to \mathbb{R}$ be a function such that $f(x) = f(x + 2\pi)$ for all $x \in \mathbb{R}$. The *Fourier series* of f is defined as

$$\sum_{n=-\infty}^{\infty} \hat{f}(n) e^{inx},$$

where $\hat{f}(n) := \frac{1}{2\pi} \int_0^{2\pi} f(x) e^{-inx} \, dx$.

Next, we introduce two important results on the uniqueness of the Fourier series. The proofs can be found in [2].

Theorem A.8. *Let f, g be measurable and integrable functions with $x \in [0, 2\pi]$ and $\hat{f}(n) = \hat{g}(n)$ for all $n \in \mathbb{Z}$. Now $f(x) = g(x)$ for all $x \in (0, 2\pi)$ where $f - g$ is continuous.*

Corollary A.9. *Let $f, g : [0, 2\pi] \to \mathbb{C}$ be continuous functions and $\hat{f}(n) = \hat{g}(n)$ for all $n \in \mathbb{Z}$. Then $f(x) = g(x)$ for all $x \in [0, 2\pi]$.*

Now we can prove an important theorem regarding the convergence of a Fourier series.

Theorem A.10. *Let $f : [0, 2\pi] \to \mathbb{C}$ be a continuous function and*

$$\sum_{n=-\infty}^{\infty} \left| \hat{f}(n) e^{inx} \right| = \sum_{n=-\infty}^{\infty} \left| \hat{f}(n) \right| < \infty.$$

Now the following equality holds

$$f(x) = \sum_{n=-\infty}^{\infty} \hat{f}(n) e^{inx}$$

where the convergence is uniform.

Proof. Since $|e^{inx}| = 1$ with all $x \in [0, 2\pi]$, we know that the series $\sum_{n=-\infty}^{\infty} \hat{f}(n)e^{inx}$ converges uniformly in $[0, 2\pi]$. Let g be the function defined as

$$g(x) = \sum_{n=-\infty}^{\infty} \hat{f}(n)e^{inx} = \lim_{N\to\infty} S_N f(x).$$

Now we know that g is continuous in $[0, 2\pi]$. Our next goal is to prove that $g(x) = f(x)$ for all $x \in [0, 2\pi]$.

Let $k \in \mathbb{Z}$. Now

$$\begin{aligned}
\hat{g}(k) &= \frac{1}{2\pi}\int_0^{2\pi} g(x)e^{-ikx} \\
&= \frac{1}{2\pi}\int_0^{2\pi} \lim_{N\to\infty} \sum_{n=-N}^{N} \hat{f}(n)e^{inx}e^{-ikx}\,dx \\
&= \lim_{N\to\infty} \hat{f}(n)\frac{1}{2\pi}\int_0^{2\pi} \sum_{n=-N}^{N} e^{inx}e^{-ikx}\,dx \\
&= \hat{f}(k),
\end{aligned}$$

Above we used the information that since the series is uniformly convergent we can change the order of integration and taking the limit. Now since both f and g are continuous and have the same fourier coefficents, by A.9 we know that $g(x) = f(x)$ for all $x \in [0, 2\pi]$. $\square$

Appendix B

Sobolev spaces

In this chapter our goal is to give the definition of a Sobolev space and some of its properties. To achieve that goal we must first define a generalization of a derivative known as the weak derivative.

First, we introduce the concept of a *multi-index* for the sake of notational convenience. An n-dimensional multi-index α is an n-tuple

$$\alpha = (\alpha_1, \alpha_2, \ldots, \alpha_n)$$

where $n \in \mathbb{N}$.

The absolute value of an n-dimensional multi-index α is defined as

$$|\alpha| = \alpha_1 + \alpha_2 + \cdots + \alpha_n$$

and is referred to as the length of a multi-index.

Given a multi-index α, we define a differential operator D^α as follows:

$$D^\alpha = \left(\frac{\partial}{\partial x_1}\right)^{\alpha_1} \cdots \left(\frac{\partial}{\partial x_n}\right)^{\alpha_n} = \frac{\partial^{|\alpha|}}{\partial x_1^{\alpha_1} \cdots \partial x_n^{\alpha_n}}.$$

Next we introduce a generalization of a derivative called the *weak derivative*. Let $u \in C^k(\Omega)$, where Ω is an open subset of $\mathbb{R}^n$ and $v \in C_0^\infty(\Omega)$. Now the following integration-by-parts formula

$$\int_\Omega D^\alpha u \phi \, dx = (-1)^{|\alpha|} \int_\Omega u D^\alpha \phi \, dx \tag{B.1}$$

holds for all $|\alpha| \leq k$ and $\phi \in C_0^\infty(\Omega)$. Notice that all terms involving integrals over the boundary of Ω, which arise in the course of integrating by parts disappear since the function ϕ and its derivatives are identically zero on the boundary of Ω.

We use the identity (B.1) as the starting point for defining the concept of weak derivative.

Definition B.2. Let α be a multi-index and $u, v \in L^1_{loc}(U)$ where $U \in \mathbb{R}^n$ is an open set. We say that v is the α:th -weak derivative of u if

$$\int_\Omega u D^\alpha \phi = (-1)^{|\alpha|} \int_\Omega v\phi$$

for all $\phi \in C_c^\infty(U)$.

We denote the α:th weak derivative of u with $D^\alpha u$. Now we can define Sobolev spaces using the definition of a weak derivative.

Definition B.3. Let $\Omega \subset \mathbb{R}^n$ be an open set, α an n-dimensional multi-index and k an integer where $0 \leq k \leq n$. The Sobolev space $W^{k,p}(\Omega)$ is defined as

$$W^{k,p}(\Omega) = \{u \in L^p(\Omega) \mid D^\alpha u \in L^p(\Omega) \text{ for all } |\alpha| \leq k\}.$$

In the special case of $p = 2$ we denote the Sobolev space $W^{k,2}(U) = H^k(U)$. We will be using this notation in the future.

Now we can define a norm for the Sobolev spaces.

Definition B.4. Let $k \in \mathbb{N}$, $1 \leq p \leq \infty$ and $u \in W^{k,p}(\Omega)$. We define the the Sobolev norm of u as

$$\|u\|_{W^{k,p}(\Omega)} = \left(\sum_{|\alpha| \leq k} \|D^\alpha u\|^p_{L^p(\Omega)} \right)^{\frac{1}{p}} \quad \text{when } 1 \leq p < \infty$$

and

$$\|u\|_{W^{k,\infty}(\Omega)} = \sum_{|\alpha| \leq k} \|D^\alpha u\|_{L^\infty(\Omega)} \quad \text{when } p = \infty.$$

The next theorem is known as *Poincaré's inequality* and will a useful tool when studying Sobolev spaces. We use the notation $(u)_\Omega$ for the average of u over Ω. More information with proof can be found in [4].

Theorem B.5. *Let $\Omega \subset \mathbb{R}^n$ be a bounded, connected and open subset with a C^1 boundary $\partial\Omega$. Assume $1 \leq p \leq \infty$. Then there exists a constant C, depending on n, p and Ω, such that*

$$\|u - (u)_\Omega\|_{L^p(\Omega)} \leq C\|\nabla u\|_{L^p(\Omega)},$$

for each function $u \in W^{1,p}(\Omega)$.

Next we define Sobolev spaces H^k for any $k > 0$. We do this by using Fourier transforms.

Definition B.6. Let $U \subset \mathbb{R}^n$ be an open set, α an n-dimensional multi-index and $k \in \mathbb{R}$ where $0 \leq k \leq n$. The Sobolev space $H^k(U)$ is defined as

$$H^k(U) = \{u \in L^2(U) \mid \int_U (1 + |\xi|^2)^k |\hat{u}(\xi)|^2 \, d\xi < \infty\}$$

where $\hat{u}$ is the Fourier transform of u.

The space $H^k(U)$, where $k > 0$ is a Hilbert space when equipped with the norm

$$(u, v)_{H^k} = \int_U (1 + |\xi|^2)^k \hat{u}(\xi)\overline{\hat{v}(\xi)} \, d\xi.$$

Next we define Sobolev spaces for negative values of k

Definition B.7. Let $U \subset \mathbb{R}^n$ be an open set, α an n-dimensional multi-index and $k \in \mathbb{R}$ where $k \leq 0$. We define the space $H^k(U)$ as the closure of $C_0^\infty(U)$ with respect to the norm $\|u\|_{H^k} = \|(1 + |\xi|^2)^{s/2}\hat{u}\|_{L^2}$

We can also give a different characterization of this space using the dual space of H^k. Consider the conjugate linear pairing

$$(u, v) \mapsto \int_U \hat{u}(\xi)\overline{\hat{v}(\xi)} \, d\xi, \text{ where } (u, v) \in C_0^\infty(U) \times C_0^\infty(U).$$

Using the Cauchy-Schwartz-inequality we get

$$\left| \int_U u(\xi)\overline{v\xi} \, d\xi \right| \leq \|(1 + |\xi|^2)^{k/2}\hat{u}(\xi)\|_{L^2} \|(1 + |\xi|^2)^{k/2}\hat{v}(\xi)\|_{L^2} = \|u\|_{H^k}\|v\|_{H^{-k}}$$

for any $k \in \mathbb{R}$.

Now if $\int u\overline{v} \, dx = 0$ for all $v \in C_0^\infty$, then $u = 0$. Therefore we can identify $H^{-k}(U)$ with the dual space of $H^k(U)$.

Next, we introduce the concept of a *trace operator* and two theorems. A more thorough study of the trace operator and proofs for the theorems can be found in [4]. The first theorem is called *the trace theorem.*

Theorem B.8. *Let $\Omega \subset \mathbb{R}^n$ be a bounded domain with a Lipschitz boundary $\partial\Omega$. Now*

(i) there exists a unique bounded linear operator $tr : H^1(\Omega) \to L^2(\partial\Omega)$ such that if $u \in C^1(\Omega \cap \partial\Omega)$, then $tr\, u = u|_{\partial\Omega}$ and

(ii) the range of tr is dense in $L^2(\partial\Omega)$.

More generally, if $u \in H^m(\Omega)$ *and* $tr_j u \equiv \dfrac{\partial^j u}{\partial \nu}$, *where* $0 \leq j \leq m-1$, *then*

$$tr_j : H^m(\Omega) \to H^{m-j-1/2}(\partial\Omega)$$

is a continuous and linear surjection.

Theorem B.9. *Let* tr *be the trace operator. Now*

$$\ker tr = H_0^1(\Omega).$$

Bibliography

[1] Mueller, J.L. and Siltanen S., 2012, *Linear and Nonlinear Inverse Problems with Practical Applications*. SIAM

[2] Astala, K. and Saksman E., 2013, *Fourier-analyysi, luentomuistiinpanot*. University of Helsinki

[3] Johnson, C., 1987, *Numerical solutions of partial differential equations by the finite element method*. Cambridge University Press

[4] Evans, L., 2010, *Partial Differential Equations*, second edition. American Mathematical Society

[5] Harikumar, R., Prabu, R. and Raghavan, S., 2013, *Electrical Impedance Tomography (EIT) and Its Medical Applications: A Review*. International Journal of Soft Computing and Engineering (IJSCE), Volume-3, Issue-4, September 2013.

[6] Ola, P., 2008, *Introduction to Electrical Impedance Tomography, luentomuistiinpanot*. University of Helsinki, Department of Mathematics

[7] Süli, E., 2012, *Notes on Finite Element Methods for Partial Differential Equations*. University of Oxford Mathematical Institute

[8] Siltanen, S., Mueller, J. and Isaacson, D., 2000, *An implementation of the reconstruction algorithm of A. Nachman for the 2-D inverse conductivity problem*. Inverse Problems, 16, pp. 681-699

[9] Sylvester, J., 1992, *A convergent layer stripping algorithm for the radially symmetric impedance tomography problem*. Communications in Partial Differential Equations, 17, pp. 1955-1994

[10] Smith, L., 2002, *A tutorial on Principal Components Analysis*. University of Otago, Department of Computer Science

[11] Wagner, T.M., 2004, *A very short introduction to the Finite Element Method*. Technical University of Munich

[12] Gisser, D.G., Isaacson, D. and Newell, J.C., 1990, *Electric current computed tomography and eigenvalues*. SIAM Journal on Applied Mathematics, 50, pp. 1623-1634

[13] Astala, K., Piiroinen, P., Tylli H.O., 2010, *Funktionaalianalyysin peruskurssi, luentomoniste*. University of Helsinki

[14] Rudin, W., 1991, *Functional analysis*. McGraw-Hill

[15] Calderón, A.P., 1980, *On an inverse boundary value problem*. Seminar on Numerical Analysis and its Applications to Continuum Physics, Sociedad Brasileira de Matematica, pp. 65-73

[16] Sylvester, J., Uhlmann, G., 1987, *A Global Uniqueness Theorem for Inverse Boundary Value Problem*. Annals of Mathematics, Vol. 125, pp. 153-169

[17] Nachman, A., 1996, *Global Uniqueness for a Two-Dimensional Inverse Boundary Value Problem*. Annals of Mathematics, Vol. 143, pp. 71-96

[18] Astala, K., Päivärinta, L., 2006, *Calderóns inverse conductivity problem in the plane*. Annals of Mathematics, Vol. 163, pp. 265-299